Optical Coordination Sensor for Precision Cooperating Robots

Wing-Choi Ma*
Electrical and Computer Engineering
Carnegie Mellon University

Alfred A. Rizzi and Ralph L. Hollis
The Robotics Institute
Carnegie Mellon University

Abstract

The need for high precision robotic systems has increased in recent years. Examples include automated assembly of complex electro-mechanical products such as disk drives, cameras, and medical devices. In this paper we present an optical sensor which can sense motion with better than 0.15 μm resolution while also offering the advantages of insusceptibility to ambient lights, high bandwidth, and a large dynamic range. The sensor is used for calibration and coordination tasks in a novel agile robotic system (minifactory) which employs cooperative 2-DOF robots. The sensor can also be used for testing, calibrating, and position sensing in many other high precision robotic applications.

1 Introduction

Our group, in the Microdynamic Systems Laboratory† is developing a rapidly reconfigurable, precise, table-top automated factory. This *minifactory*, part of a larger framework called "Agile Assembly Architecture," is intended to improve the assembly of complex electro-mechanical products [1]. Minifactory uses cooperative 2-DOF robots (Fig. 1). Overhead z, θ *manipulator* robots work in conjunction with planar x, y *courier* robots to perform 4-DOF assembly tasks. The courier robots float on a tabletop surface (*platen* ensemble) and are responsible for transporting sub-assemblies through the factory. Manipulators, mounted on bridges which are connected to base units of the minifactory, pick parts from local feeders and place them into the sub-assemblies. Replacing the traditional 4-DOF SCARA robots with cooperative 2-DOF robots yield advantages in compactness, precision, and modularity [2].

Courier robots and the platen surface form a system of planar motors. The platen serves as the stator and the courier as the rotor. The platen surface has an array of fine square teeth. A precision magnetic platen sensor [3] built in to each courier measures its position on the platen surface with a resolution of 200 nm (1σ), enabling closed-loop servo control [4].

Since there is no linkage between the pair of independent 2-DOF robots (courier and manipulator), a sensor was needed which could measure the robots' relative positions with micron level precision. The subject of this paper is the development of an optical coordination sensor to perform this task. The optical sensor system, as shown in Fig. 1, uses a light emitting diode (LED) to define the location of the overhead manipulator. A sensor module which is fixed on the courier can then determine the position of the LED. The following section describes the theory and design of the sensor module. The optical sensor is based on a position-sensitive photodiode (see, *e.g.*, [5]). Whereas these devices have been used in many similar applications, this paper presents a complete design and unique application to modular robotics. Section 3 concentrates on the signal processing and electronics aspect of the system. Section 4 gives experimental measurements and calibration results. Section 5 is the summary and conclusion.

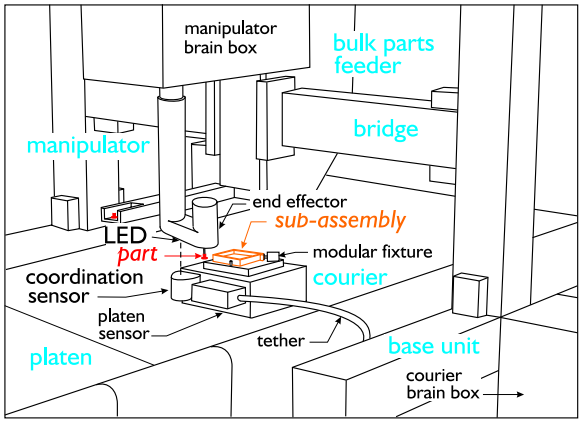

Figure 1: Elements in a minifactory and the optical coordination sensor carried by couriers.

2 Physical Design

The physical design of the optical coordination sensor is shown in Fig. 2. The assembled sensor has dimensions of $31 \times 36 \times 35$ mm (W × L × H). It comprises an infra-red LED, absorption filter, lens, position sensitive detector (PSD), machined parts, and circuit boards. Infra-red light emitted from the LED passes first through the absorption filter, strongly attenuating extraneous visible or ultra-violet light coming from the environment. The lens collects the ir light and projects the image of the LED onto the surface of the PSD. The PSD detects the cen-

*Currently at GE Medical Systems, 3000 N. Grandview Blvd, Waukesha, WI 53188.

†http://www.cs.cmu.edu/~msl.

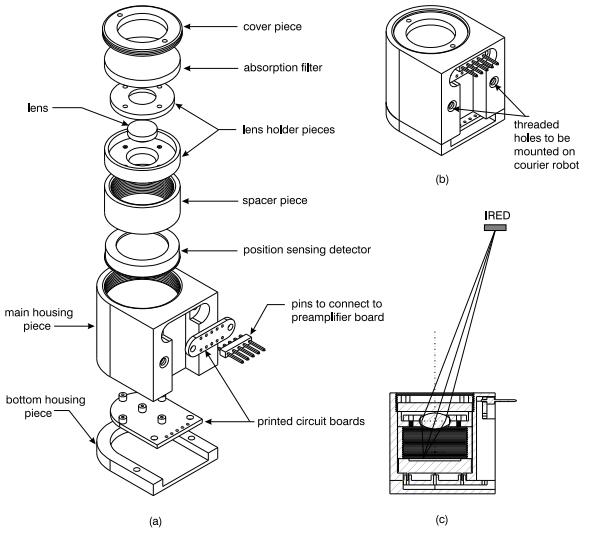

Figure 2: (a) Exploded view of the optical coordination sensor, (b) general view of the assembly, (c) optical ray diagram.

troid position of the light spot shining on its surface. The circuit boards and wires redirect current signals from the PSD to pins connected to preamplifier circuits.

The heart of the optical sensor is a duolateral super linear position sensitive detector, model DL10 from UDT Sensors, Inc. Its operation is based on the semiconductor lateral photoeffect as shown in Fig. 3. The PSD is composed of a continuous precision sensing surface. The top side of this surface is an ion implanted p-type layer, and the bottom is an ion implanted n-type layer. When light is absorbed by the photodiode, electron-hole pairs are induced at the incident position. Electrons migrate to the n-type region and holes to the p-type region. The electrons and holes are collected by pairs of parallel electrodes on the corresponding layer. Both the n-type and p-type layers are resistive surfaces which are highly uniform. The photocurrent collected by each of the two electrodes on a layer is inversely proportional to the distance between the incident light position and the electrode. This relationship is governed by

$$I_O = I_{X1} + I_{X2}, \tag{1}$$

$$I_{X1} = I_O \cdot (\frac{\frac{L}{2} + x}{L}), \tag{2}$$

$$(I_{X1} - I_{X2}) = I_O \cdot (\frac{2x}{L}). \tag{3}$$

In addition, x, which is the displacement measured from the center of the two parallel electrode plates to the light incident position (in the direction of X1), can be calculated using

$$x = (\frac{I_{X1} - I_{X2}}{I_{X1} + I_{X2}}) \cdot \frac{L}{2}. \tag{4}$$

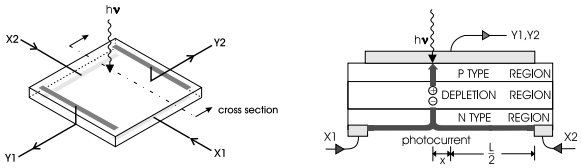

Figure 3: (a) Topology of a Duolateral PSD, (b) theory of operation.

One attractive feature of Eq. (4) is that the resulting position information is independent of both the intensity of the light spot and the quantum efficiency of the PSD. Stated another way, Eq. (4) is independent of I_O and depends only on the "centroid of power density" of the light spot. This greatly simplifies the design of the optical system, which can simply be treated (to first order) as a pin-hole camera.

Off-the-shelf components were carefully selected for the optical sensor system. For the LED, a high-reliability, high-power infra-red emitter was used. This LED, an OD-50J from Opto Diode Corp., has a peak emission wavelength which matches the wavelength where the PSD has its highest responsivity. Another important requirement is a uniform light intensity distribution over a wide solid angle. This allows the light spot imaged onto the PSD to have a uniform and constant light energy distribution, and keeps I_O in Eq. (1) relatively constant as the LED moves across the optical sensor. This constancy improves the precision and resolution of the spot's position information. The lens used in the sensor module is a symmetric convex, synthetic fused silica lens with a multi-layer anti-reflection coating. Synthetic fused silica has a thermal expansion coefficient which is 15 times smaller than glass, higher ir transmission, and increased hardness. The lens coating minimizes "ghost images" which can appear on the PSD surface from internal reflections in the sensor housing. Finally, the diameter of the lens is relatively large to maximize the amount of collected light.

Machined parts and circuit boards were designed using CAD software. Two lens holder pieces were made to hold and keep the lens aligned with the center of the PSD. The top piece was made of Delrin^{TM} to provide some compliance in holding the fragile lens. The bottom piece was made of aluminum, and was black anodized to minimize spurious reflections in the sensor housing. Next to the lens holder is the spacer piece which sets the distance between the lens and the PSD. Thread-like cuts were made on its inner surface and the spacer was black anodized. These black trenches trap and absorb light which reaches its surface. The sensor housing itself has three pieces: the main housing piece, the cover piece, and the bottom piece. Finally, there are two

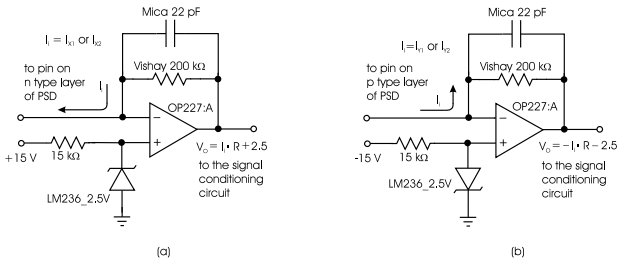

Figure 4: Transimpedance amplifier with (a) +2.5V (b) -2.5V for the reverse bias of the PSD.

circuit boards inside the housing, connected by five wires. The large circuit board aligns the axes of the PSD and transfers the output currents from the PSD to the wires, and the small circuit board hosts the external connector pins and redirects the PSD output currents to the preamplifiers.

3 Electronic Design

It is important to note that the position information from the optical sensor is calculated after a chain of electronic circuits which process the sensor signals. There are circuits to 1) amplify the PSD currents and convert these currents to voltages (preamplifiers), 2) perform signal conditioning, 3) do the analog difference and sum, and finally 4) to digitize the resulting signals. To maximize the signal-to-noise ratio, the electronics were carefully designed and built to be highly stable and accurate.

The preamplifier circuitry is located adjacent to the optical sensor. Low offset, low noise operational amplifiers were used. They are connected in the transimpedance configuration as shown in Fig. 4. The first function of the circuit is to reverse-bias the duolateral PSD, which reduces its junction capacitance, improving frequency response. The second function of the circuit is to convert the low-level output currents from the PSD to high-level voltages. Very precise and stable resistors are required for this task. Vishay S102C series 0.01% low noise resistors were chosen. Finally, the small capacitor across the feedback path of the transimpedance amplifier is used to prevent gain peaking due to the stray parasitic capacitance presented in the inverting input of the operational amplifiers.

Some interfering light (*e.g.*, sunlight, ceiling 120 Hz fluorescent tubes) inevitably gets past the optical filter and is imaged onto different locations on the PSD. These spurious images fool the PSD into giving false information about the true position of the LED light spot. This is avoided by ac modulating the LED signals, so that erroneous signals which are not modulated can be electronically eliminated. To accomplish this, the LED is switched on and off with equal durations at a selected frequency (5 kHz was used in our system). The demodulation technique used to condition the output signals from the preamplifiers is illustrated in the Matlab Simulink model shown in Fig. 5. This detection scheme provides both noise immunity and speed. Basically, the input signal is multiplied by a square wave with the same phase as the input signal and having a magnitude varying from -1 to 1 V. The resulting signal is low-pass filtered to obtain a dc output which conveys the information from the PSD. This demodulation scheme is good at filtering low-frequency signals such as fluorescent and incandescent lamps, sunlight, dark current from the PSD, and ripple on the bias voltage for the PSD. It is important to notice that the 8^{th}-order low-pass filter is formed by cascading four 2^{nd}-order Butterworth filters. This design was chosen for its "maximally flat" characteristic, and the cascade approach was chosen over a single 8^{th}-order Butterworth design for its faster settling time. A simple zero-crossing detection scheme is used to recover the clock signal. This is preceded by a high-pass filter is to remove the dc offset and some slow-varying noise in its input. The zero-crossing detection is done with a comparator.

The "balanced" demodulator is the crucial element in the synchronous detection scheme. It must be fast, and be able to provide a well-matched and stable gain of ± 1. This was made possible by using the AD630BD from Analog Devices. The chip has two front-end precision operational amplifiers, and a comparator which is responsible for selecting the active amplifier. Furthermore, it has internal laser-trimmed thin film resistors which are very accurate and temperature stable. For the low pass responses in the demodulation scheme, a unity gain Sallen-Key low-pass realization [6] was chosen for simplicity, and the fact that its dc gain is always equal to one, independent of variations in the values of the passive components. This is important since resistor and capacitor values vary with environmental conditions. If the dc filter gain is sensitive to the environment, the precision and stability of the position information from the PSD would be lost.

Implementation of the clock recovering circuit is shown in Fig. 6. The first part of the circuit is an inverted summing amplifier. The high pass filter is implemented with a simple capacitor and resistor network connected to the comparator's high-impedance inverting terminal. The output transistor of the comparator operates in the saturated mode. Its emitter is connected to ground, and its collector is pulled up to 5 V through a resistor, making the output CMOS compatible. The comparator is configured to have a zero threshold with a small hysteresis.

In reality, the sensor output signals have finite asymmetric rise and fall times. These imperfections result in a regenerated clock signal which is time delayed from the actual clock signal, and has

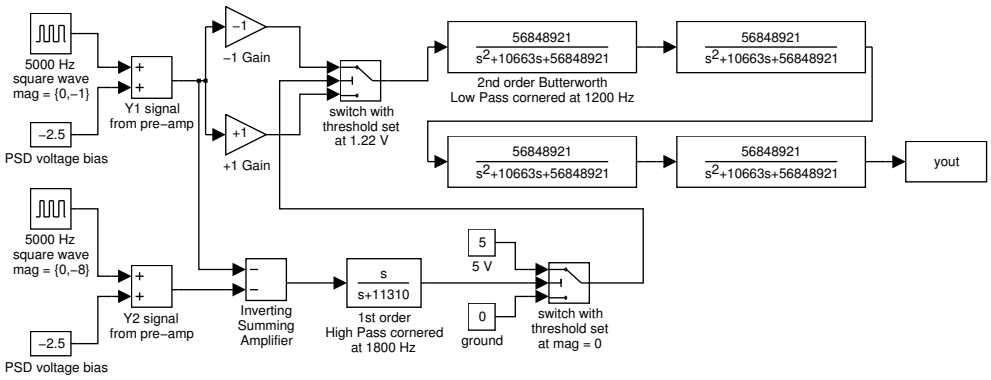

Figure 5: Matlab Simulink block diagram of the synchronous detection scheme.

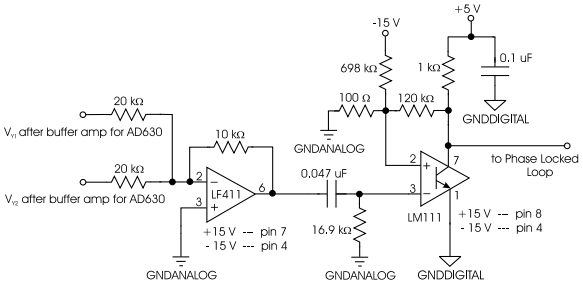

Figure 6: High pass filter and voltage comparator.

an asymmetric duty cycle. The effect of the time delay is cancelled out by the normalization step in Eq. (4). On the other hand, the asymmetry in the duty cycle of the regenerated clock is a problem since a recovered clock signal with a perfect 50% duty cycle is required for the signal conditioning scheme to provide complete immunity to slowly varying input noises. To correct this problem, a phase locked loop (PLL) circuit is placed after the comparator. The MM74HC4046N PLL from National Semiconductor is used. It has a phase comparator which uses only the positive rising edges of the input signal and is insensitive to the duty cycle of the input signal. A detailed description of the PLL's operation is shown in Fig. 7. The comparator has a tri-state output which is fed to an external filter network. The output of the filter is connected to the high-impedance input of the voltage controlled oscillator (VCO) input. Therefore, the filter network simply stores charge to hold voltage. When in lock, the rising edges of the VCO and the signal input have a phase difference of zero. The VCO output signal, which has a 50% duty cycle and the same frequency and phase as the input signal, is then used to control the demodulator circuit.

Another important part of the signal conditioning circuit is the differencing operation required by Eq. (4). The PGA205BP precision pin-programmable gain instrumentation amplifier from Burr Brown was used. It has tightly matched, stable, internal resistors to achieve a high common-

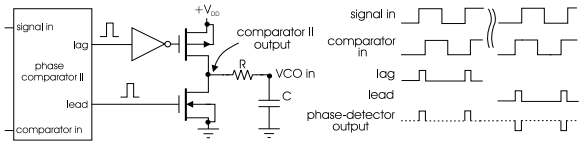

Figure 7: Phase detector II in HC4046

mode rejection ratio. The other advantage of this device is its programmable gain, permitting selection of the desired resolution of the sensor by changing gains of 1, 2, 4, and 8 V/V.

There was a great deal of attention to detail in the electronics construction to prevent noise from coupling into the system. Noise reduction techniques used included careful layout of the printed circuit board, design of a stable and low-noise power supply circuit, decoupling of IC amplifiers, careful selection of passive components, and shielding of the cables and housing. These techniques can minimize the noise sources, eliminate the noise coupling channels, and/or make the receivers less sensitive to noise pick up [7].

4 Experimental Results

Many experiments were run to measure the performance of the optical coordination sensor. The sensor module and its preamplifier circuit board were translated under a fixed LED by a two-axis precision linear stage having a minimum step size of 1 μm. The vertical distance between the LED and the top of the sensor housing was held at 25 mm. Therefore, the magnification factor, or the ratio between the object distance and the image distance, was about 2.5. An IP-16ADC analog to digital converter (A/D) from GreenSpring Computer was used to read the sensor. The IP-16ADC has an internal 16-bit A/D chip which calibrates itself with a highly stable and precise voltage reference during each power up cycle with a typical accuracy of ± 1 Least Significant Bit (LSB). Finally, there was plenty of room light in the environment. A bright fluorescent lamp was less than two feet away, to test the sensor's immunity to ambient lights.

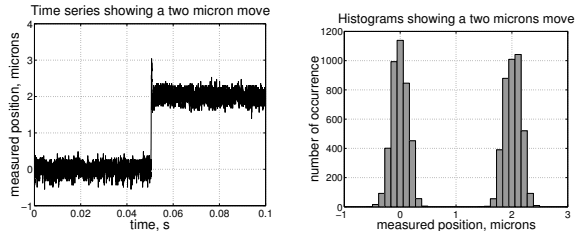

Figure 8: Time series and histogram plots for a 2 μm move (Gain of 8).

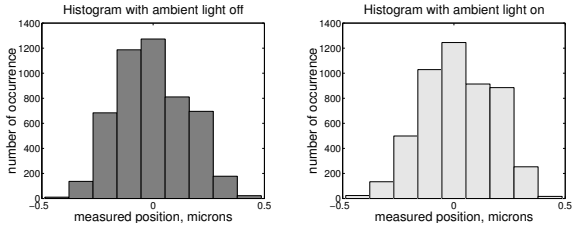

Figure 9: Histograms of signal (gain of 8) when the ambient 120 Hz fluorescent light was either off (left) or on (right).

4.1 Resolution measurements

To test the resolution of the optical coordination sensor near the center region of the PSD, the gain of the instrumentation amplifiers was set to 8 and the stage was moved to a position where the sensor read zero on both axes. The stage was then commanded to move 2 μm in one of its axes, between sensor readings. The axis of the PSD and the axis of the stage were well aligned. Figure 8 shows both the time series and histogram plots of the sensor readings. The sensor position readings were converted to the actual movement of the stage in μm, and the standard deviations (1σ) for both data sets before and after the move were 0.15 μm. With the magnification ratio of 2.5, the standard deviation of the position measurement of the light spot on the 10 mm $\times$ 10 mm PSD surface was 60 nm. This resolution can still be improved. For example, if the averaging is done in software, the zero mean Gaussian noise presented in the data can be reduced (at the expense of bandwidth). Also, if the intensity of the LED is increased, I_O in Eq. (1) and the resolution increases (at the expense of range). The intensity of the LED, however, can only be increased to a level that does not saturate the PSD. This same experiment was repeated with the instrumentation amplifier gain set at 2. In this case, the standard deviation (1σ) for the data was 0.35 μm. It is important to note that the standard deviation was only slightly higher than the 0.15 μm result obtained with a gain of 8 in the difference amplifier. One reason is that noise which was less than 1 LSB of the A/D at a gain of 2 became detectable when the gain was increased to 8.

The follow-up experiment was to test the effect of ambient light on the sensor system. Both the fluorescent desk lamp and the overhead room light were turned on and off. Sensor data were taken to record the relative change in the position measurements. Figure 9 shows histograms for the two data sets. The standard deviation of both data remained at 0.15 μm. There were no changes due to the ambient lighting condition, verifying the sensor's immunity to ambient light.

In practice, there are non-ideal characteristics in the system. These include things like the tilting of the PSD, tilting of the sensor housing, image distortion caused by the lens, non-linearity of the PSD, misalignment of the PSD axes with the stage's axes, and gains introduced by the analog electronics. These affect the precision in measuring the planar position of the LED. The next set of experiments was performed to test the linearity of the sensor system. The sensor was moved in discrete steps of equal distance, and the corresponding sensor outputs were recorded at each location after the stage had settled. The left plot in Fig. 10 shows the sensor position reading in both X and Y axes when the instrumentation amplifier gain was set at 2 and the stage was moving in steps of 1000 μm. Each point in the plot is an average of 1000 data points. The maximum range has not been reached by the stage, but as shown in the figure, the sensor system had a range of better than 21 mm $\times$ 21 mm. The right plot shows the result of another experiment, with identical settings, except that the instrumentation amplifier gain was set to 8 and the stage was programmed to move in incremental steps of 140 μm. This plot is the "zoom in" version of the previous plot, with the scale on both axes multiplied by a factor of four.

Detailed bandwidth measurements on the sensor system have not yet been performed, but appear to be in the range of several hundred Hz, wide enough to be viable in the minifactory application, and potentially effective in many other areas.

4.2 Calibration

The sensor must be calibrated to measure the planar position of a point in space to micron-level accuracy due to inherent non-linearities. Part of the data in the graph shown in the left plot of Fig. 10 was used as the initial data for an interpolation scheme. The rest of the data in the graph served to test the scheme. The Matlab function `ZI=GRIDDATA(X,Y,Z,XI,YI,'cubic')` was used to perform 2D surface fitting of the form `Z=F(X,Y)` to the data in the non-uniformly spaced vectors `(X,Y,Z)`. `X` and `Y` were the position readings of the sensor for the initial data, and `Z` was the corresponding motor's x axis (or y axis) location. `GRIDDATA` then interpolated this surface at the points specified by `(XI,YI)` to produce `ZI`. The term "cubic"

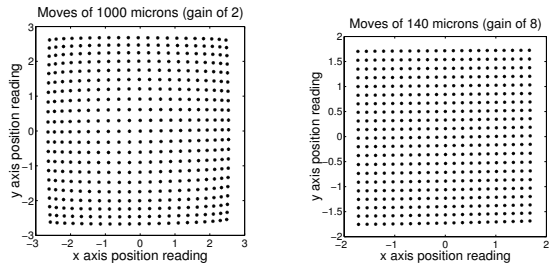

Figure 10: Linearity plot for (left) gain of 2, (right) gain of 8.

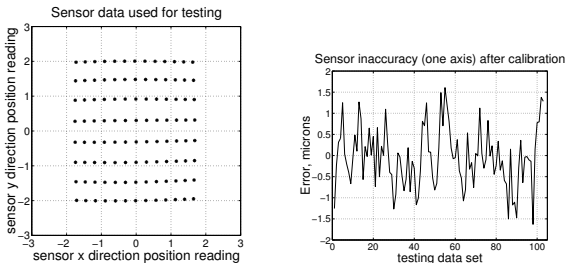

Figure 11: (Left) data set used for testing, (right) error between the actual movement of the courier robot and the interpolated movement for the testing set.

denotes a cubic interpolation based on Dalaunay triangulation to the non-uniform input data set. However, the algorithm to do the `GRIDDATA` routine on-line requires a considerable amount of computational time. Therefore, the values of the surface, as calculated by `GRIDDATA`, were stored in a look-up table. Values in between the index points are evaluated using a bilinear interpolation scheme. The two-dimensional input space was divided into a grid of 100×100 equally spaced points. The plot in the left of Fig. 11 shows the data used for the testing of the calibration scheme and the plot on the right shows the error between the actual location of the sensor and its location calculated on-line from the look-up table. After calibration, the sensor is accurate to the μm level in a range of about 20 mm with the initial data points 1000 μm apart from each other. Finally, we note that the interpolated surface can also be scaled (and optionally offset) to compensate for an LED moving to a different height. The scaling factor required can be obtained from a height measurement calibration of the sensor, and heights can be measured accurately by the sensor module (with the help from the courier robot) using triangulation.

5 Conclusions

The design, building, and testing of a precision optical coordination sensor system for our minifactory is presented. Experimental results show that the sensor has sub-micron resolution, and micron level accuracy, while having a wide dynamic range (tens of millimeters), high bandwidth (several hundred Hz), and insusceptibility to ambient lights. We are continuing work to more accurately characterize the sensor's bandwidth.

Applications of the sensor in the minifactory environment includes kinematic identification and calibration of the overhead manipulator, requiring cooperation between the manipulator and the courier. The derived kinematic information is important in order to realize the inherent precision of the pair of 2-DOF robots in doing cooperative assembly tasks. In dozens of experiments, a minifactory courier and manipulator have successfully performed vision-guided cooperative assembly of small medical devices, after automatic factory calibration using this coordination sensor [8]. Typical calibrations are in the sub-micron range. We are working to further characterize system-level performance.

Additionally, we have built in provisions for overlaying data modulation on the 5000 Hz LED carrier frequency, allowing courier robots to "read" identification serial numbers of manipulators and other types of minifactory manufacturing equipment.

Acknowledgements

This work and Wing-Choi Ma were supported by NSF grant DMI-9527190.

References

[1] A. A. Rizzi, J. Gowdy, and R. L. Hollis, "Agile assembly architecture: An agent-based approach to modular precision assembly systems," in *IEEE Int'l. Conf. on Robotics and Automation*, (Albuquerque), pp. 1511–1516, April 1997.

[2] A. E. Quaid and R. L. Hollis, "Cooperative 2-DOF robots for precision assembly," in *Proc. IEEE Int'l Conf. on Robotics and Automation*, (Minneapolis), May 1996.

[3] Z. Butler, A. A. Rizzi, and R. L. Hollis, "Integrated precision 3-DOF position sensor for planar linear motors," in *IEEE Int'l Conf. on Robotics and Automation*, (Leuvan, Belgium), pp. 3109–3114, May 1998.

[4] A. E. Quaid and R. L. Hollis, "3-DOF closed-loop control for planar linear motors," in *IEEE Int'l Conf. on robotics and Automation*, (Leuven, Belgium), pp. 2488–2493, May 1998.

[5] D. J. Noorlag and S. Middlehoek, "Two-dimensional position-sensitive photodetector with high linearity made with standard I.C. technology," *Solid State and Electron Devices*, vol. 3, no. 3, pp. 75–82, 1979.

[6] S. Franco, *Design with Operational Amplifiers and Analog Integrated Circuits*. McGraw-Hill, 1988.

[7] H. Ott, *Noise Reduction Technique In Electronics Systems*. John Wiley and Sons, 1976.

[8] M. L. Chen, S. Kume, A. A. Rizzi, and R. L. Hollis, "Visually guided coordination for distributed precision assembly," in *IEEE Int'l Conf. on Robotics and Automation*, (San Francisco), April 2000.